Adsorptive Separation of CO_2 in Sulfur Functionalized Nanoporous Carbons

Dipendu Saha[1,*], Gerassimos Orkoulas[1], Jihua Chen[2], Dale K. Hensley[2]

[1] Department of Chemical Engineering,
Widener University, One University Place, Chester, PA 19013
[2] Center for Nanophase Materials Sciences, Oak Ridge National Laboratory. Oak Ridge, TN 37831, USA

*Corresponding author's E-mail: dsaha@mail.widener.edu , Phone: +1 610 499 4056, Fax: 610 499 4059 (D. Saha)

To be submitted to *Langmuir*

Abstract

In this research, we have synthesized two sulfur functionalized nanoporous carbons by post-synthesis modifications with sulfur bearing activating agents that simultaneously enhanced the surface area and introduced sulfur functionalities on the carbon surface. The Brunauer–Emmett–Teller (BET) surface areas of these materials were 2865 and 837 m^2/g with total sulfur contents of 8.2 and 12.9 %, respectively. The sulfur-functionalized carbons were characterized with pore textural properties, X-ray photoelectron spectroscopy (XPS), thermogravimetric analysis (TGA) and electron microscopy (SEM and TEM). In both the carbons, CO_2 adsorption isotherms and kinetics were measured in three different temperatures of 298, 288 and 278 K and pressures up to 760 torr. The gravimetric CO_2 uptake followed the trend with BET surface area but the surface area-based uptake was reversed and it followed the trend of sulfur content. The heat of adsorption of CO_2 in low uptake was 60-65 kJ/mol, which is the highest for CO_2 adsorption in porous carbons. In order to investigate the adsorptive separation of CO_2, N_2 and CH_4 adsorption isotherms were also measured at 298 K and 760 torr. The selectivity of separation for CO_2/N_2 and CO_2/CH_4 was calculated based on the Ideal Adsorbed Solution Theory (IAST) and all the results demonstrated the high CO_2 selectivity for the carbon with higher sulfur content. The adsorption isotherms were combined with mass balances to calculate the breakthrough behavior of the binary mixtures of CO_2/N_2 and CO_2/CH_4. The simulation results demonstrated that the dimensionless breakthrough time is a decreasing function of the mole fraction of CO_2 in the feed stream. The overall results suggest that the sulfur-functionalized carbons can be employed as potential adsorbents for CO_2 separation.

1. Introduction

In today's perspective, there is an overwhelming need for separation of CO_2 from flue or post-combustion gas mixtures. The primary source of post-combustion CO_2 release can be attributed to coal, oil and natural gas that are composed of 80 % of CO_2 release worldwide[1]. Amongst these sources, coal powered electricity generation plants release maximum amount of CO_2, contributing to 41% and 60% of CO_2 in U.S. and world, respectively[2]. The anthropogenic CO_2 emission has increased 80% in 2004 compared to previously recorded values and its concentration in atmosphere has exceeded the value of 390 ppm, which is higher than any value recorded in modern times[3]. According to International Panel on Climate Change (IPCC), the expected temperature rise[3] at the end of 21st century is within 1.8 to 6.4 °C and the major part of it is contributed from the anthropogenic greenhouse gas emission including CO_2. Separation of CO_2 from the flue gas stream is part of the carbon capture and sequestration (CCS) plan in which the captured CO_2 is either injected into different geological formations for permanent sequestration or employed as feedstock for other chemicals. The other need for separation of CO_2 is for the enrichment of natural gas (methane, CH_4) as a part of the gas sweetening process to meet pipeline quality standard or consumer requirement. For entrapment of CO_2 from coal based power plants or for gas sweetening, alkanolamine is the current technology for post-combustion CO_2 capture. However, this process is quite expensive and associated with different types of hazards. For coal power plants that utilize alkanolamine technique, the total energy penalty rises to 30% of the total output[1] and 70% of the total cost of CCS is contributed to the CO_2 separation unit.

Adsorptive separation, especially pressure swing adsorption (PSA) is an alternative process for CO_2 separation. It provides the advantage of inexpensive and sustainable separation process compared to chemical separation. The key challenge for utilizing adsorptive separation is to employ a suitable adsorbent with high selectivity for CO_2 compared to other gases that are often present . For post-combustion CO_2 separation, the most common impurity that is often mixed with it is nitrogen (N_2) and therefore, a high CO_2/N_2 selectivity is required. For natural gas sweetening, CO_2 needs to be selectively separated from methane. Different kinds of adsorbents, including nanoporous carbons[4,5] zeolites[6,7,8,9], silica[10,11,12] or Metal-Organic Frameworks (MOFs)[3,13] have successfully demonstrated their potential role in CO_2 separation from N_2 or CH_4. The details of CO_2 capture by adsorbent materials have been described in several review articles[3,13,10,14,15,16,17,18]. In order to investigate the preferential CO_2 adsorption from the gas mixture and owing to the difficulty in performing mixed gas adsorption, the selectivity and breakthrough behavior are obtained from pure-component adsorption data using simple thermodynamic models (such as Ideal Adsorbed Solution Theory-IAST) and mass balances.

Hetero-atom doped nanoporous carbons, mostly, B, N, S or P-doped carbons have gained lot of interest in today's perspectives owing to their different applications catalysis or energy storage[19],[20]. Sulfur doping is one unique approach of heteroatom doping and provides several remarkable features to the host carbon. Unlike other heteroatoms, a sulfur atom is much larger compared with boron or nitrogen, so it protrudes out of the graphene plane, thereby creating an uneven surface with unique properties, such as superconductivity[21],[22] as revealed in the theoretical studies. Other than structural defects, the lone pair of electrons in a sulfur atom induces polarizability and interactions with oxygen[20]. In the field of CO_2 adsorption, Xia et al.[23] reported an elevated CO_2 adsorption amount of 2.4 mmol/g at 25 °C on sulfur doped nanoporous carbons. The heat of adsorption was in the range of 59 kJ/mol near zero loading which was one of highest values ever reported for carbon-based materials. Seema et al.[24] reported even higher CO_2 uptake amount of 4.5 mmol/g at 25 °C at ambient pressure in reduced graphene oxide/polythiophene complex. Recently, Bandosz et al.[25],[26] reported the chemical interactions between sulfur doped carbons and CO_2. Despite there are several reports on CO_2 adsorption on sulfur doped nanoporous carbons, the two drawbacks of the current works are *(a)* The sulfur doped nanoporous carbons were synthesized either from sulfur bearing polymers or some fine chemicals, like graphene which possesses an arduous task of scale-up to synthesize in bulk quantity, and *(b)* In the past studies, only CO_2 adsorption characteristics were reported, but not the selectivity of separation of CO_2 from other gases or breakthrough plots. In this article, we report a simple technique of synthesizing sulfur doped nanoporous carbons that is easy to scale-up and calculate the selectivity of CO_2 separation from N_2 and CH_4. Furthermore, we calculate the dimensionless breakthrough time associated with a pressure swing adsorption (PSA) process.

2. Experimental

2.1 Synthesis of sulfur functionalized nanoporous carbons

To synthesize the sulfur doped carbon, we have modified the procedures reported by Liu and Antonietti[27]. The synthesis protocol requires two-steps, the synthesis of pure carbon and the simultaneous activation and sulfur functionalization. The synthesis of the pure nanoporous carbon is very similar to that of our previous publications[28],[29],[30],[31],[32]. Typically, 5 g of resorcinol and 4.3 g of Pluronic F127 were dissolved in solvent mixture composed 20 mL water and 30 mL ethanol. After they are dissolved, 0.5 mL 36% HCl was added as catalyst and stirred for over an hour. Then, 36% 4.8 mL formaldehyde solution was added as cross-linking agent and stirred for 3 days. The polymer layer is subsequently separated from the solvent and transferred to a Lindburg-Blue tube furnace for carbonization. In carbonization, the sample was heated to 100 °C at a ramp rate of 10

°C/min, then up to 400 °C at 2°C/min, and finally up to 1000 °C at 5°C/min. All the carbonization steps and cooling profiles were performed in nitrogen atmosphere.

In order to insert sulfur functionality and further activation of pure carbon, sodium thiosulfate ($Na_2S_2O_3$) was employed as the activating agent. Typically, solid sodium thiosulfate and carbons were mixed in 1:1 and 4:1 ratio in a lab-scale blender and heated in a tube furnace up to 800 °C at 10°C/min in nitrogen atmosphere and cooled in the same fashion. The sample was removed from the furnace, washed in DI water several times for 24 hours and then overnight (?). Throughout the manuscript, the sulfur doped carbons that were produced with 1:1 and 4:1 ratios of sodium thiosulfate to carbons are termed as CS-1 and CS-2, respectively.

2.2 Materials Characterization

Both types of sulfur-doped carbons were characterized with x-ray photoelectron spectroscopy (XPS), pore textural properties, thermogravimetric analysis (TGA), and electron microscopy (SEM and TEM). XPS analyses were performed in a Thermo-Fisher K-alpha instrument XPS system operating at monochromatic Al K-α as an x-ray anode. The intensity of x-ray energy was 1486.6 eV and the resolution was 0.5 eV. The pore textural properties including BET surface area, differential and cumulative pore size distributions were calculated from nitrogen adsorption-desorption experiments at 77 K and ambient pressure in Quantachrome's Autosorb-iQ instrument. Pore size distribution data were obtained by using non-local density functional theory (NLDFT) in the instrument's built-in software. Thermogravimetric analysis (TGA) was performed in TA instruments' SDT Q600 instrument. Scanning electron microscopic images were obtained in a Carl Zeiss Merlin SEM microscope operating at 30 kV. As a part of SEM imaging system, the energy dispersive X-ray (EDX) results were obtained with a system from Bruker Nano GmbH using an XFlash detector 5030. TEM images were captured in Carl Zeiss Libra 120 TEM operating at 120 kV.

2.3 Adsorption experiments

All the adsorption experiments were obtained in the Quantachrome's Autosorb-iQ instrument up to ambient pressure (760 Torr) and varying temperature (278 to 298 K). An external Julabo temperature controller with a 1:1 mixture of propylene glycol and water as chilling fluid controlled the temperature for all the adsorption experiments except liquid nitrogen temperature (77 K). The preciseness of the temperature controller was within ±0.1 °C of the set point. All the adsorbate gases were of ultra-high purity grade and obtained from commercial source (Air-Gas).

3. Results and Discussions

3.1 Materials characteristics

The qualitative and quantitative analyses of surface functionalities were obtained by XPS studies of S-*2p* analysis (figure 1) and the results are shown in table 1. The total sulfur content in CS-1 and CS-2 are 8.2 and 12.9%, respectively. The key sulfur functionalities are C=S, C-S, S=O-C and SOx, with the highest functional group being the C-S group in both carbons. As per XPS results, the actual sulfur content may be slightly higher than reported value, as there are two overlapping regions between S-O and C-O groups and C-S-C/C-SH functionality and C-*1s* peaks. Therefore, three additional sulfur bearing functionalities, including S-O, C-S-C and C-SH may also be present in these samples, which were not possible to distinctively identify thorough XPS analysis. CS-1 and CS-2 have 5.4 and 8.6 % S-O/C-O groups, respectively. Besides that, CS-1 and CS-2 have 8.9 and 20.1% of oxygen, respectively with approximately 1% sodium in each that might have originated from sodium thiosulfate. From the XPS studies, it is evident that higher ratio of sodium thiosulfate in the synthesis stage resulted in higher sulfur content in the resultant carbons. The total sulfur contents in these two materials are higher than most of the sulfur-doped carbon materials synthesized from sulfur containing precursors, proteins or other sulfur bearing compounds, like thiophene or hydrogen sulfide[33]. However, this amount is lower than that of reported by Liu and Antoinette[27] (~30 %). The key reason for having such a low sulfur content may be attributed to the fact that these authors[27] employed glucose as the carbon source unlike a porous carbon in our study. At elevated temperature, glucose itself has a lower carbon or char yield compared to porous carbon and hence these numbers may not provide a one-to-one comparison with respect to the starting carbon materials.

The degree of burn off (B.O.) in CS-1 and CS-2 are 55% and 24.5%, respectively, upon treating with sodium thiosulfate at elevated temperature. Interestingly, higher ratio of sodium thiosulfate resulted in lower degree of burn off, which is in contrary to the normal circumstances and opposing the remarks made by Liu and Antonietti[27]. Such opposing trend may be attributed to the non-stoichiometric reactant mixtures or inhomogeneous mixing. As mentioned earlier, a direct comparison with the results from Liu and Antonietti[27] is also difficult owing to the different natures of carbon precursors. Nitrogen adsorption-desorption plots at 77 K for both CS-1 and CS-2 are shown in figure 2(a). Both the isotherms are of Type IV according to IUPAC classifications with the hysteresis loop showing the capillary condensation in the mesopores. The BET specific surface areas are 2865 and 837 m^2/g for CS-1 and CS-2 respectively, which directly follows the trend in degree of burn off. Pore size distribution of both the samples are obtained combining the NLDFT calculations from nitrogen adsorption at 77 K and CO_2 adsorption at 273 K, while employing CO_2 adsorption results for narrow micropore regions only. The pore size distribution results are shown in figure 2(b). Both CS-1 and CS-2 have micropore widths in the regions of 3.5, 4.8 and 15.4 Å, while the mesopore width lies within 40 to 45 Å. The total pore volume of CS-1 and CS-2 are 2.3 and 0.71 cm^3/g respectively. To the best

of our knowledge, the BET surface area of CS-1 (2865 m^2/g) is probably higher than most of the sulfur functionalized nanoporous carbons, except that of reported by Liu and Antonietti[27]. The higher BET surface area possessed by most of the sulfur-doped carbons are in the range of 1100 m^2/g[33]. CS-2 possessed the lower BET surface owing to lower degree of burn off as mentioned earlier. However this BET surface area is still higher than several other sulfur doped carbons produced from sulfur containing protein or polymeric materials[33].

SEM and TEM images of CS-1 and CS-2 are shown in figure 3. TEM images did not reveal an ordered structure or porosity, only graphitic ribbons were partly observed. SEM image of CS-2 revealed an ordered porosity in the structure as observed in figure 3(d). The top arrow on the left side of the fig 3(d) shows the network of channel-like structures, which are the side view of the mesopore passages. Similar arrow on the right hand side of the figure shows the opening or mouth of the mesopores that are arranged in orderly fashion. Such ordering of mesopore networks were not observed for CS-1, most likely higher degree of bun off destroyed the ordered mesoporosity. The inset views of the SEM images (fig 3b and 3d) represent the EDX mapping for sulfur. According to EDX results, sulfur percent in CS-1 and CS-2 and 7.55 to 9.53% and 12.52 to 13.9% respectively, which are very close to that of obtained in XPS results.

Thermogravimetric analysis (TGA) of the sulfur doped carbons in air and nitrogen plots are shown in figure 3. The decomposition peaks of both the carbons were in the range of 500 °C with an apparent slightly higher peak area of CS-1 compared to CS-2 suggesting a greater mass loss for CS1. The inset figure that demonstrates the TGA under nitrogen reveals several peaks, with three prominent peaks at 245 and 675 °C regions. CS-1 has a larger peak at 975 °C, whereas CS-2 has a series of smaller peaks at 660 to 874 °C. These peaks most likely belonged to the decomposition of sulfur and oxygen functionalities from the carbon materials.

3.2 Adsorption results

Figure 5(a) and (b) show the CO_2 adsorption uptake for CS-1 and CS-2, respectively, at the three different temperatures of 278, 288 and 298 K and pressure up to 760 Torr. The overall uptake of CO_2 is always higher for CS-1 in all the temperatures. The highest CO_2 adsorption amounts at 278 K are 3.16 and 2.82 mmol/g for CS-1 and CS-2, respectively. At ambient temperature (298 K), the CO_2 uptakes were 2.06 and 1.81 mmol/g for CS-1 and CS-2, respectively. The adsorption of CO_2 onto these sulfur-doped carbons may be attributed to both physisorption and a stronger reactive interaction between CO_2 and sulfur functionality as suggested by Seredych et al.[26] In the nanosized pores, the sulfur embedded onto the aromatic rings enhances the CO_2 adsorption by acid-base interactions. Additionally, sulfonate and sulfoxide groups can attract CO_2 by polar interactions. Hydrogen bonding between acidic groups and on the carbon surface and CO_2 may also

influence CO_2 adsorption[26]. The highest CO_2 uptake in our work is slightly lower than that of reported by Xia et al.[23], (maximum 2.4 mmol/g) and almost of half of that of reported by Seema et al[24] (maximum 4.5 mmol/g). The lower pure component CO_2 adsorption compared to that of previously published sulfur-doped carbons might be attributed to the lower micropore area in our carbons compared to the reported materials. From figure 2(b), it is evident that these carbons have a very significant amount of mesopore volume. It is also well known that narrow micropores are most optimal for CO_2 adsorption. It is possible that the larger mesopore volume did not take part in the adsorbing CO_2 and therefore, overall CO_2 uptake remained lower compared to the purely microporous carbons. In order to further compare the CO_2 adsorption in two of our sulfur-doped carbons, we have calculated the specific surface area (SSA) based CO_2 adsorption with BET surface area as the reference (figure 6). At 756 torr and 298 K, CO_2 uptake in CS-1 and CS-2 are 7.19×10^{-4} and 2.16×10^{-3} mmol/SSA, respectively. Clearly, CO_2 adsorption amount is one magnitude high in CS-2 compared to CS-1 and it can be attributed to the higher sulfur content in CS-2.

Figure 5(b) and (c) show the kinetics of CO_2 adsorption at the same temperatures of 278, 288 and 298 K for CS-1 and CS-2, respectively. In these figures, m_t is the mass adsorbed at time t and m_∞ is the saturation mass. It is evident that adsorption kinetics in CS-1 is sluggish compared to CS-2; it took about 100 to 120 seconds to reach the reached saturation level in CS-1 unlike CS-2 that reached the saturation within 50 to 60 seconds. The slow kinetics in CS-1 may be attributed to its higher microporosity. It is also observed that the kinetics became slightly more sluggish with the decrease in temperature that suggests the adsorption is an energetically activated process. In order to model the kinetics, we have employed pseudosecond equation that fit with the experimental kinetics plot with 99% of regression fit. The pseudosecond order equation is given by[34]

$$\frac{dq_t}{dt} = k_2(q_{e,2} - q_t)^2 \qquad (1)$$

where, $q_t, q_{e,2}$ and k_2 are uptake amount at time t, equilibrium uptake and pseudosecond order equilibrium constant, respectively. Integration of above equation yields to

$$\frac{t}{q_t} = \frac{1}{k_2 q_{e,2}^{\ 2}} + \frac{t}{q_{e,2}} \qquad (2)$$

The pseudosecond order equilibrium constant (k_2) can be calculated from the linear plot of t versus $\frac{t}{q_t}$. The equilibrium constant can be related to temperature through an Arrhenius type equation given by

$$k_2 = k_{2o} \exp\left(-\frac{E_a}{RT}\right) \qquad (4)$$

where E_a is the activation energy. The pseudosecond order model constants (k_2) are shown in table 2 for CS-1 and CS-2 in three different temperatures of 298, 288 and 278 K. The activation energies (E_a) for CS-1 and CS-2 are 8.3 and 15.4 kJ/mol, respectively. The higher activation energy for CS-2 compared to CS-1 probably suggests a stronger interaction of CO_2 with CS-2. It is also important to note that surface area based CO_2 adsorption in CS-2 was one order of magnitude higher than CS-1 although the gravimetric CO_2 adsorption was higher in CS-1. Higher activation energy validates the stronger interaction between CO_2 and CS-2 and the higher surface area based CO_2 adsorption. For the micropore diffusion, the kinetic model involving the diffusivity can be calculated by the equation[35],[36],

$$1-\left(\frac{m_t}{m_\infty}\right) = \frac{6}{\pi^2}\exp\left(\frac{-\pi^2 D_c t}{r_c^{\,2}}\right) \qquad (5)$$

where, D_c is the intracrystalline diffusivity and r_c is the intracrystalline radius. $D_c / r_c^{\,2}$ is referred to as diffusive time constant. The diffusive time constant ($D_c / r_c^{\,2}$) can be calculated by the linear regression of t versus $\ln\left(1-\frac{m_t}{m_\infty}\right)$ within 70% to 99% of the value. In this study, the diffissive time constants were shown in table 2 for CS-1 and CS-2 in three temperatrues of 298, 288 and 278 K. The higher diffusive time constants of CS-2 support its faster kinetics.

From the isotherms at these three temperatures, we have calculated the heat of adsorption by using the Van't Hoff equation, given by,

$$\frac{\Delta H}{RT^2} = -\left(\frac{\partial \ln P}{\partial T}\right)_a \qquad (6)$$

where ΔH is the enthalpy or heat of adsorption, P is pressure and T is temperature and a is the adsorption amount. Integrating Van't Hoff equation,

$$\frac{\Delta H}{RT} = \ln P + C \qquad (7)$$

where C is constant of integration. From the set of isotherms at three different temperatures, a series of isosteres are generated and from the slope of isosteres, the heat of adsorption is calculated. Heat of adsorption values is shown in figure 7. It is observed that the heat of adsorption of the both the carbons are in similar range. In the higher uptake or higher-pressure range, the heat of adsorption lies within 20-30 kJ/mol. In the region of

very low adsorption, these carbons demonstrate very high heat of adsorption values of 60-65 kJ/mol. Probably, these values are higher than that of all other porous carbons and very similar to that of sulfur-doped carbons reported by Xia et al[23].

In order to compare CO_2 adsorption with other gases, we have employed two most common gases that need to be separated from CO_2, and these are methane (CH_4) and nitrogen (N_2). The adsorption isotherms are shown in figure 8(a) and (b) for CS-1 and CS-2, respectively. As observed for most of the porous materials including carbons, CO_2 adsorption amount was always highest followed by CH_4 and N_2. The CH_4 uptake amounts were in the range of 0.93 to 0.74 mmol/g and nitrogen demonstrated the lowest uptake of 0.29 to 0.25 mmol/g. It is clear that, similar to that of CO_2 uptake, CH_4 and N_2 uptake amounts were also the direct functions of BET surface area.

The equilibrium selectivity ($\alpha_{1/2}$) of component 1 (stronger adsorbate, CO_2) over component 2 (weaker adsorbate, CH_4 or N_2) is defined as[37]:

$$\alpha_{1/2} = \frac{x_1 / y_1}{x_2 / y_2} \tag{8}$$

where x and y are the mole fractions in adsorbed phase and bulk gas phase, respectively. The most common and popular way of calculating selectivity from adsorption isotherms is the Ideal Adsorbed Solution Theory (IAST), originally proposed by Myers and Prausnitz[38]. Figure 9(a) and (b) show the selectivity for CO_2/N_2 and CO_2/CH_4, respectively as a function of mole fraction of CO_2. The highest CO_2/N_2 selectivity was in the range of 50 to 60 in very low mole fraction of CO_2, whereas the CO_2/CH_4 selectivity was much lower, in the range of 6-7 in the lowest CO_2 mole fraction. All the CO_2 selectivity plots have a minimum at around 0.2 mole fraction of CO_2 and then it started to increase again. It is also noteworthy to mention that CS-2 possesses a greater CO_2 selectivity compared to that of CS-1, despite the fact that pure component adsorption amount of each of the three gases including BET surface area were higher for CS-1. Therefore, this result clearly demonstrates that BET surface area and pure component isotherms may not dictate the equilibrium selectivity. In this case, higher sulfur content of CS-2 and interaction of sulfur with CO_2 might have influenced the selectivity parameters.

For pressure swing adsorption, it is also useful to calculate adsorption selection parameter ($S_{1/2}$) given by[6,37]

$$S_{1/2} = \frac{\Delta q_1}{\Delta q_2} \alpha_{1/2} \tag{9}$$

where Δq_1 and Δq_2 are the differences in adsorption capacity (working capacity) at adsorption pressure and desorption pressure for component 1 and 2, respectively. In order

to calculate the adsorption selection parameter ($S_{1/2}$), we set the adsorption and desorption capacity at 1 bar and 0.1 bar, respectively. Adsorption selection parameter as a function of selectivity is shown in the secondary axes of figure 9(a) and (b). It is obvious that selection parameters are also higher for CS-2 compared CS-1.

In order to further investigate the efficiency of the materials as potential adsorbents for CO_2 separation, we have also developed a simple methodology that can be used to determine the breakthrough behavior of all binary mixtures studied. Consider flow of a binary gaseous mixture of species 1 and 2 through a column which is packed with adsorbent material. It is assumed that species 1 is the strong adsorbate (CO_2) compared to 2 (N_2 or CH_4). Furthermore, it is assumed that flow through the column resembles that of plug flow, the column is kept at isothermal conditions, and the pressure drop is negligible. Diffusion and mass transfer effects from the gas phase to the adsorber surface are also neglected. Thus, the gas phase, which is assumed to be an ideal gas, is always at thermodynamic equilibrium with the adsorbed phase. Under these simplifying approximations, the adsorption process through the column can be described by a set of two first-order partial differential equations[37],[39] , namely a mass balance for species 1

$$\frac{\partial C_1}{\partial t}+\frac{\partial\left(uC_1\right)}{\partial z}+\frac{1-\varepsilon}{\varepsilon}\rho\frac{\partial q_1}{\partial t}=0 \qquad (10)$$

as well as a total mass balance

$$C\frac{\partial u}{\partial z}+\frac{1-\varepsilon}{\varepsilon}\rho\frac{\partial q}{\partial t}=0 \qquad (11)$$

where C_j s the concentration of species j, $C=C_1+C_2=p/RT$ is the total concentration, u is the gas-phase velocity, ε is the column porosity, and ρ is the skeletal density of the solid material. The moles of species j adsorbed per unit adsorber volume, q_j, and the total moles, $q=q_1+q_2$, are found from thermodynamic equilibrium relations (such as IAST). At fixed temperature T, and pressure p, the amounts adsorbed are functions of C_1 i.e., $q_1=q_1\left(C_1\right)$ and $q=q\left(C_1\right)$. Solution of the system of equations (10) and (11) yields the concentration at position z within the column at time t. As material is deposited through the column the composition of the gas-phase changes and the gas-phase velocity u is, therefore, different from that at the inlet, u_0.

Straightforward manipulation of (10) and (11) yields the following expression for the gas-phase velocity

$$\ln\left(\frac{u}{u_0}\right)=\int_{C_1(0,t)}^{C_1(z,t)}\frac{\frac{1-\varepsilon}{\varepsilon}\frac{\rho}{c}q'}{1+\frac{1-\varepsilon}{\varepsilon}\rho\left(q_1'-q'\frac{C_1}{C}\right)}dC_1 \qquad (12)$$

where the prime signifies derivative with respect to C_1. Using the previous expression for u, the mass balance (10) can be cast in the following form

$$\frac{\partial C_1}{\partial t} + u_C \frac{\partial C_1}{\partial z} = 0 \qquad (13)$$

with

$$u_C = \frac{u}{1 + \frac{1-\varepsilon}{\varepsilon}\rho\left(q_1' - q'\frac{C_1}{C}\right)} \qquad (14)$$

If an inlet condition $C_1(0,t) = f(t)$ is specified, the solution of (13) is of the form[37,40] $C_1(z,t) = f(t - z/u_C)$. The inlet condition usually corresponds to a step function input (i.e., $f(t) = C_{10}H(t)$ where $H(t)$ is the unit step function). In that case, the outlet concentration, $C_1(L,t)$, will also be a step function characterized by a time lag t_{break}, given by

$$\frac{u_0 t_{break}}{L} = 1 + \frac{1-\varepsilon}{\varepsilon}\rho\left(q_1' - q'\frac{C_{10}}{C}\right) \qquad (15)$$

which provides an estimate of the "breakthrough" time required to achieve separation of the binary mixture. For the case for which the pure-component isotherms are linear functions and the binary adsorption equilibrium can be described by IAST, the derivatives q_1' and q' are constants. For all other cases the derivatives must be evaluated numerically. In this work, the dimensionless breakthrough time defined as[39] $\tau = u_0 t_{break}/\varepsilon L$ has been calculated for all the binary systems under consideration.

Figure 10(a)-(d) show the breakthrough plots for CO_2 in the mixture of CO_2/N_2 and CO_2/CH_4 in CS-1 and CS-2 with a condition of inlet mole fraction of[39] CO_2 as 0.15 in all the cases. Based on the analysis, it is evident that the actual breakthrough time (t_{break}) for CO_2 in both CO_2/N_2 and CO_2/CH_4 mixture would be higher for CS-1 under the same condition of bed length, inlet velocity and bed porosity. Such longer breakthrough time in CS-1 may be attributed to the higher working capacity or essentially the higher adsorption uptake of CO_2 as observed in figure 8. The dependency of the breakthrough time on the inlet mole fraction of CO_2 is shown in figure 11. The overall trend suggests that the breakthrough time decreases with the increase in mole fraction of CO_2 as the bed becomes saturated quickly with the elevated level of CO_2 in the feed stream. For both the binary mixtures of CO_2/N_2 and CO_2/CH_4, the difference in breakthrough time between CS-1 and CS-2 remains similar except for CO_2/N_2 when the CO_2 mole fraction is very low ($<10^{-3}$). The other distinct feature that can be observed from these plots is that the breakthrough time of CO_2 in CO_2/N_2 system decreases more sharply compared to that of CO_2/CH_4. Such difference may be attributed to the dissimilar interference in adsorption between N_2 and CH_4 in presence of CO_2 and difference in shapes of N_2 and CH_4 isotherms.

4. Conclusions

In this work, two sulfur-doped nanoporous carbons were synthesized by activating the resorcinol formaldehyde derived porous carbons with sodium thiosulfate in different ratios. The activation resulted in the dual results of incorporation of sulfur bearing functional groups onto the nanoporous carbons and enhancement of pore textural properties. The sulfur contents in the carbons were 8.2 and 12.9%, where the major sulfur containing groups were C-S, C=S, S=O-C and SO_x. Gravimetric CO_2 adsorption at the three temperatures of 298, 288 and 278 K confirmed the dependence of CO_2 adsorption on BET surface area but surface area-based CO_2 adsorption showed the dependence on sulfur contents of carbons. The kinetics of CO_2 adsorption fitted well with pseudosecond order model where the high activation energy (calculated based on temperature dependent pseudosecond order rate constant) for high sulfur bearing carbon demonstrated its stronger interactions with CO_2 molecules. The heat of adsorption of CO_2 in low adsorption amount was 60-65 kJ/mol, which was highest for the porous carbons and is in the range of other sulfur-doped carbons reported in literature. In order to compare the separation of CO_2 adsorption with other gases and calculate the selectivity of adsorption, CH_4 and N_2 adsorption were also reported at 298 K, and for both the materials, CO_2 adsorption was always higher. The selectivity of separation for CO_2/N_2 and CO_2/CH_4 was calculated based on Ideal Adsorbed Solution Theory (IAST). The breakthrough plots for the gas pairs of CO_2/N_2 and CO_2/CH_4 were simulated by using mass balance and selectivity of separation. It was found that breakthrough time for CO_2 increases with the increase in its mole fraction in the feed stream.

Acknowledgement

This work is partly supported by American Chemical Society sponsored Petroleum Research Fund (ACS-PRF, Grant Number 54205-UNI10). D. Saha also acknowledges the start-up funding from School of Engineering (SOE), Widener University. TEM (J.C.) and SEM (D.K.H.) experiments were partially conducted at the Center for Nanophase Materials Sciences, which is a DOE Office of Science User Facility.

Table 1. Characteristics of sulfur content

Content/functionality (%)	**CS-1**	**CS-2**
Total sulfur (excluding S-O, C-O, C-S-C, C-SH)	8.2	12.9
C=S	0.2	0.3
C-S	5.1	7.4
S=O-C	0.9	0.9
SOx	1.9	4.3
S-O/C-O	5.4	8.6
Total carbon content	82.9	67
Total oxygen content	8.9	20.1

Table 2. Pseudosecond order rate constant (k_2) and diffusive time constants (D_c / r_c^2) for CS-1 and CS-2

Adsorbent	**Parameters**	**T=298 K**	**T=288 K**	**T=278 K**
CS-1	k_2 ($mmol^{-1}s^{-1}$)	1.70	1.40	1.33
	D_c / r_c^2 (s^{-1})	$4.19x10^{-3}$	$3.21x10^{-3}$	$2.81x10^{-3}$
CS-2	k_2 ($mmol^{-1}s^{-1}$)	3.97	3.82	2.56
	D_c / r_c^2 (s^{-1})	$9.02x10^{-3}$	$8.79x10^{-3}$	$5.79x10^{-3}$

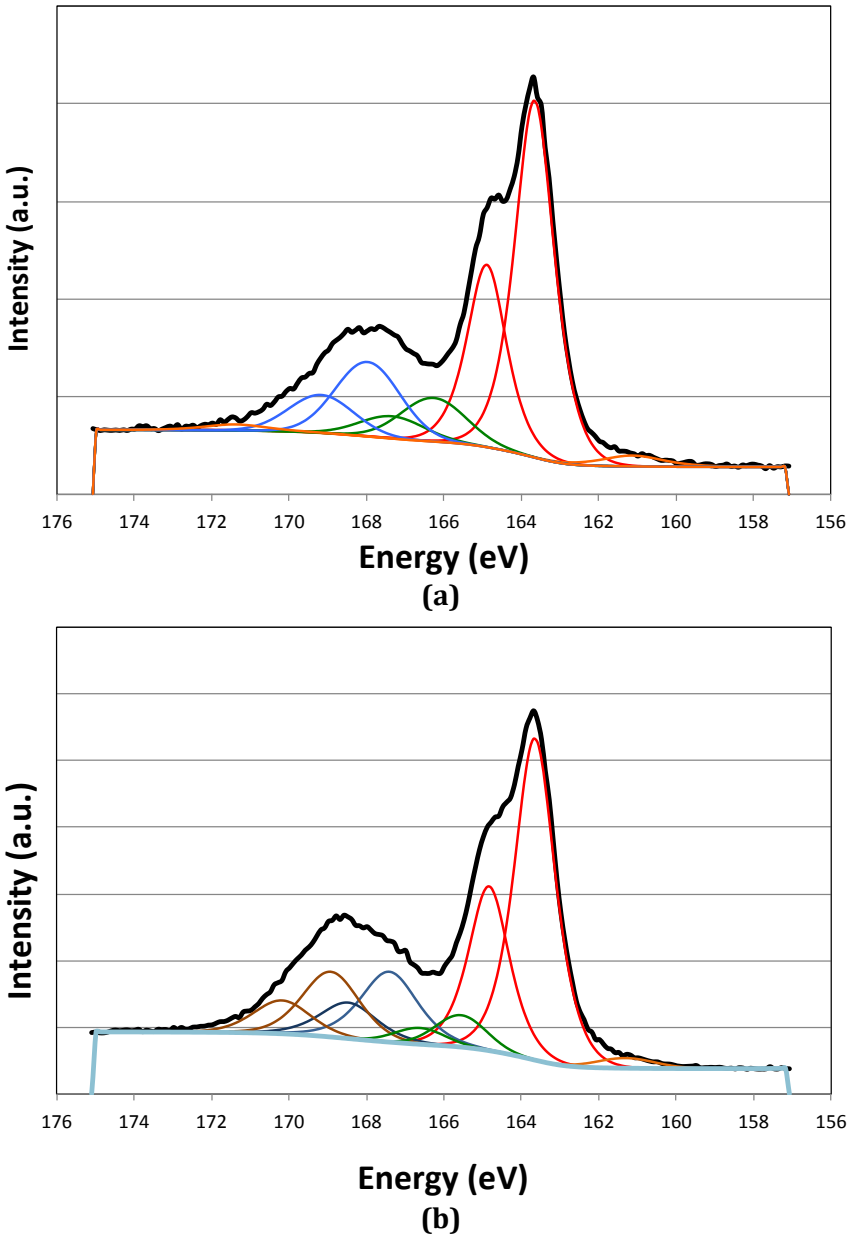

Figure 1. XPS spectra of CS-1 (a) and CS-2 (b)

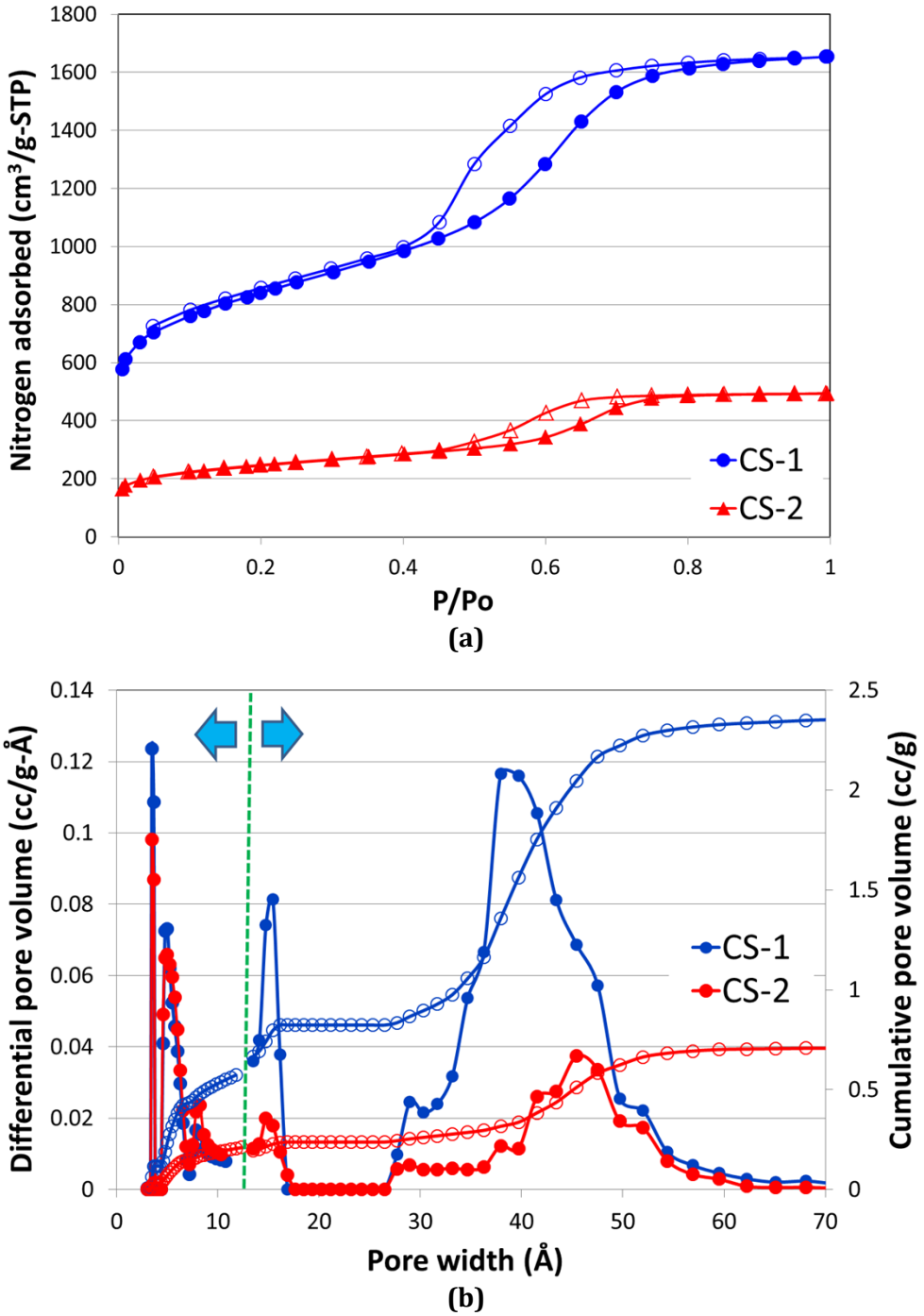

Figure 2. Nitrogen adsorption-desorption plot at 77 K (a), Pore size distribution (PSD) obtained by non-local density function (NLDFT) theory calculations (b). The PSD was calculated by CO_2 adsorption at 273 K (left-side arrow) and N_2 adsorption at 77 K (right-side arrow). The open and closed symbols are for cumulative and differential pore size distributions, respectively.

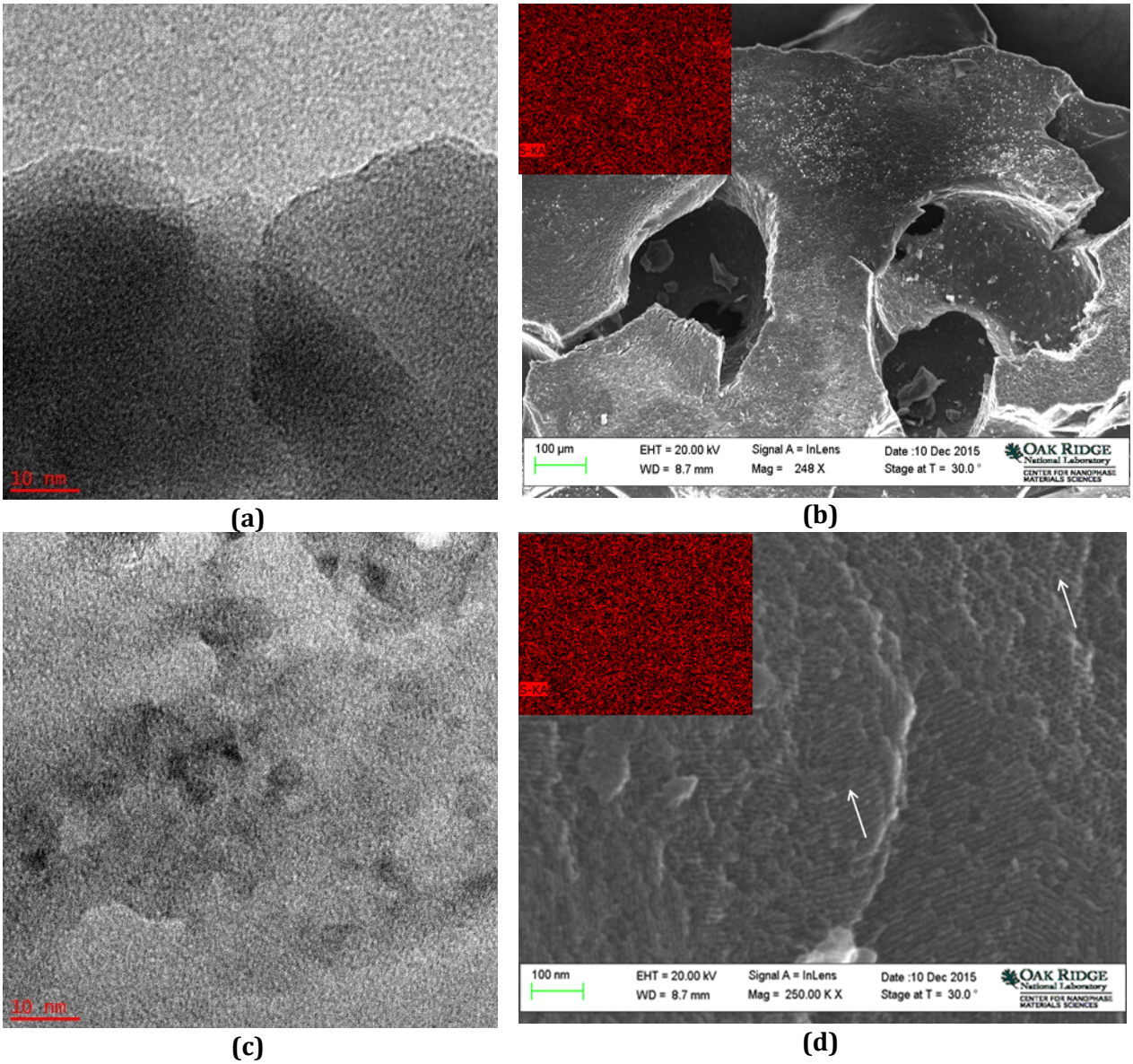

Figure 3. SEM and TEM images of CS-1 (a and b), and CS-2 (c and d). The inset images of fig (b) and (d) show the EDX mapping for sulfur. The arrows in fig (d) indicate the ordered porosity in CS-2. The left arrow show the channel (side-view) of the mesopore while the right arrow show the opening of the mesopore.

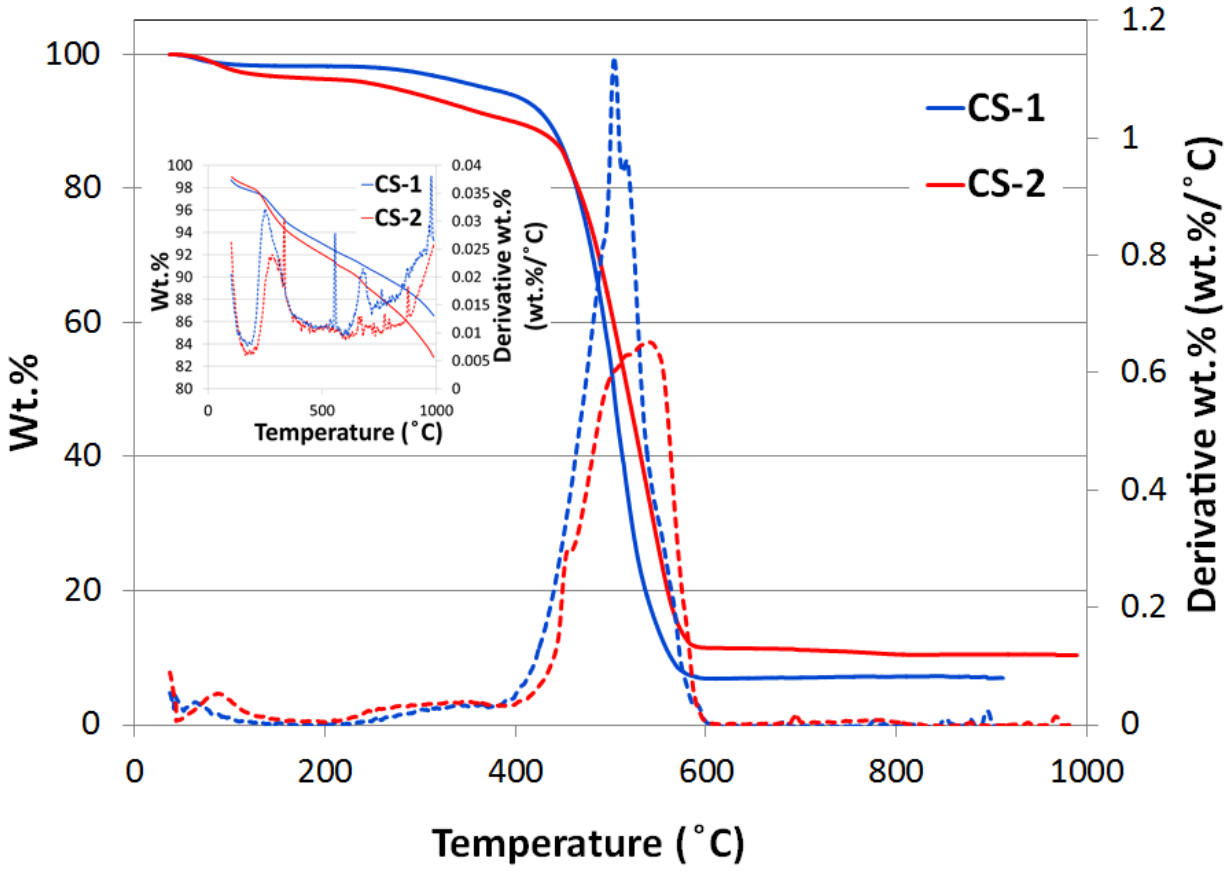

Figure 4. Results of thermogravimetric analysis (TGA) of CS-1 and CS-2 in air. The inset plot shows TGA in Nitrogen. The dotted lines represent the derivative wt.% values

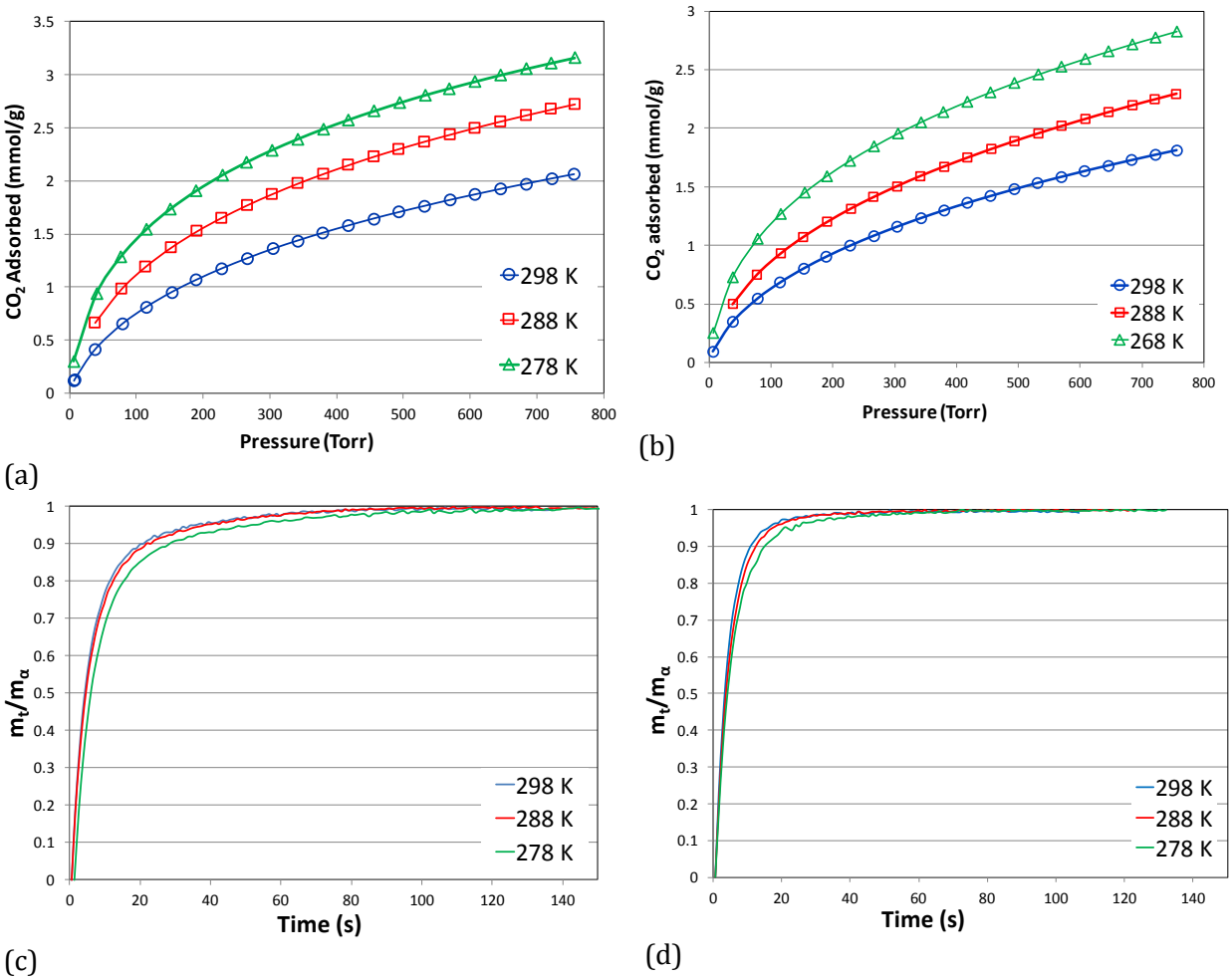

Figure 5. CO_2 adsorption isotherms in three temperatures of 298 K, 283 K and 268 K in CS-1 (a) and CS-2 (b). CO_2 adsorption kinetics in CS-1 (c) and CS-2 (d)

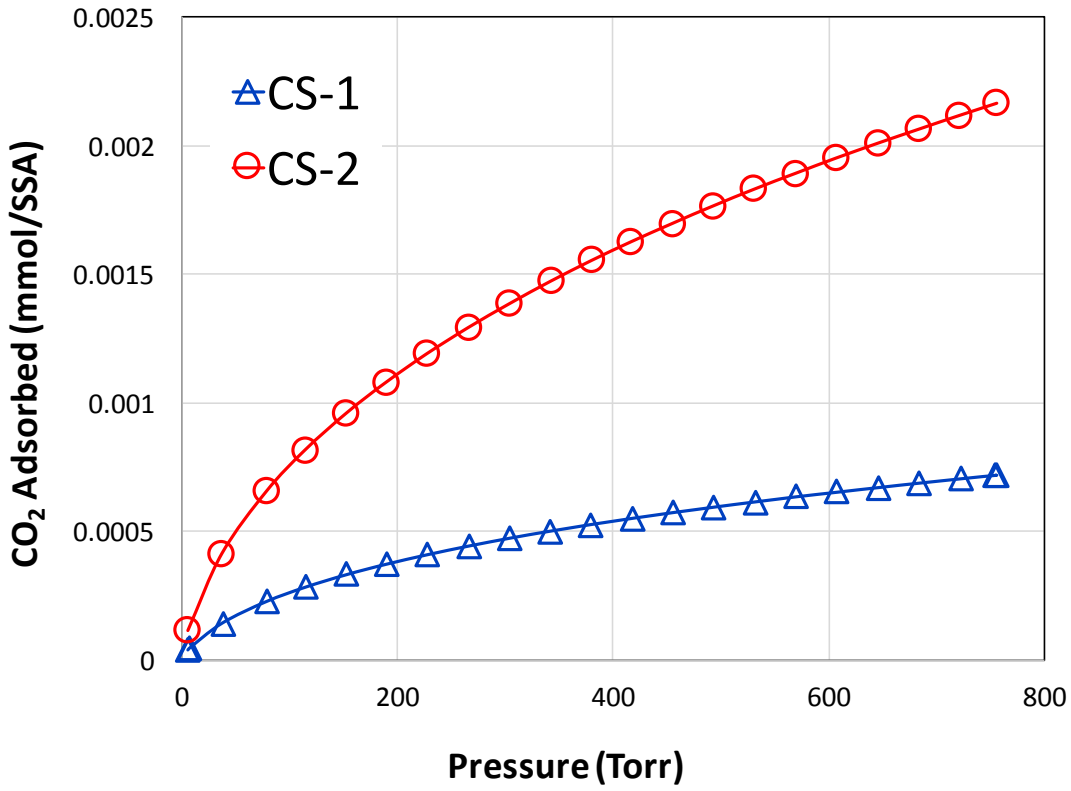

Figure 6. Specific surface area (SSA) based CO2 adsorption in CS-1 and C-2 at 298 K. BET surface area was employed as the reference SSA.

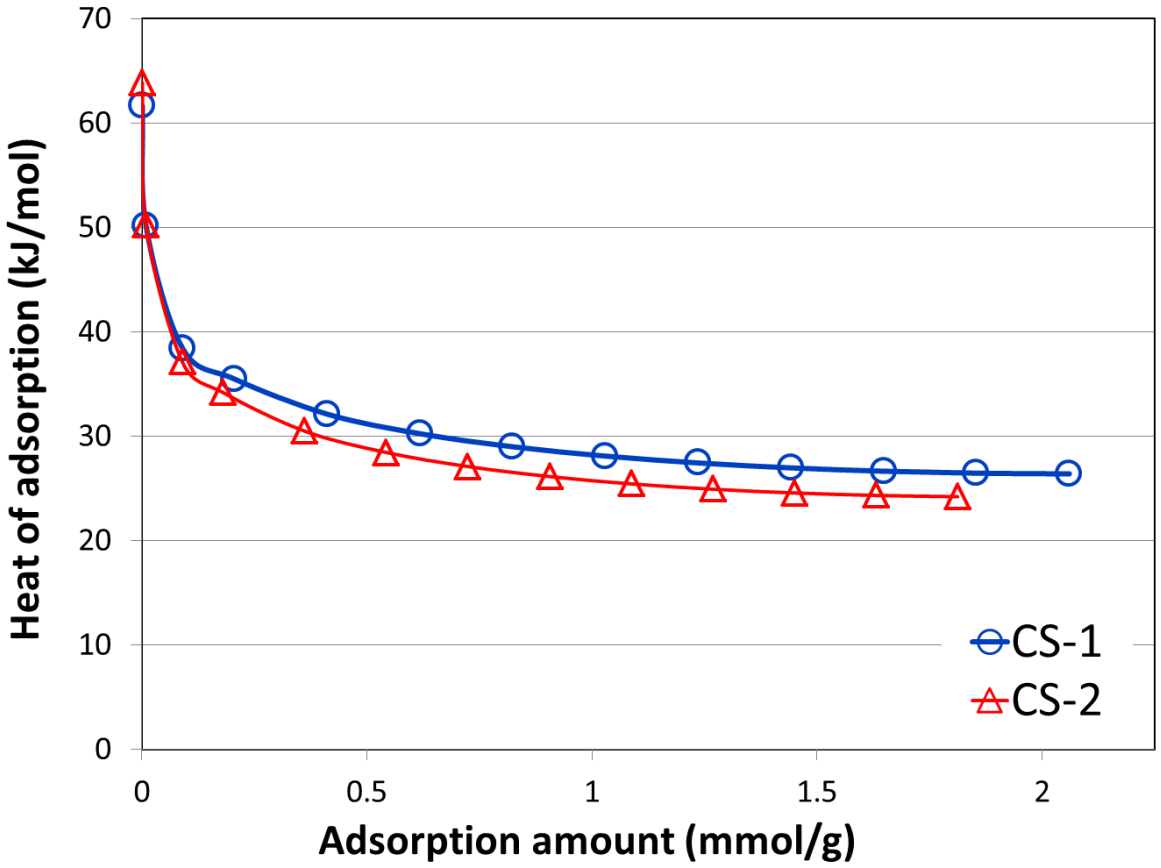

Figure 7. Heat of CO_2 adsorption in CS-1 and CS-2

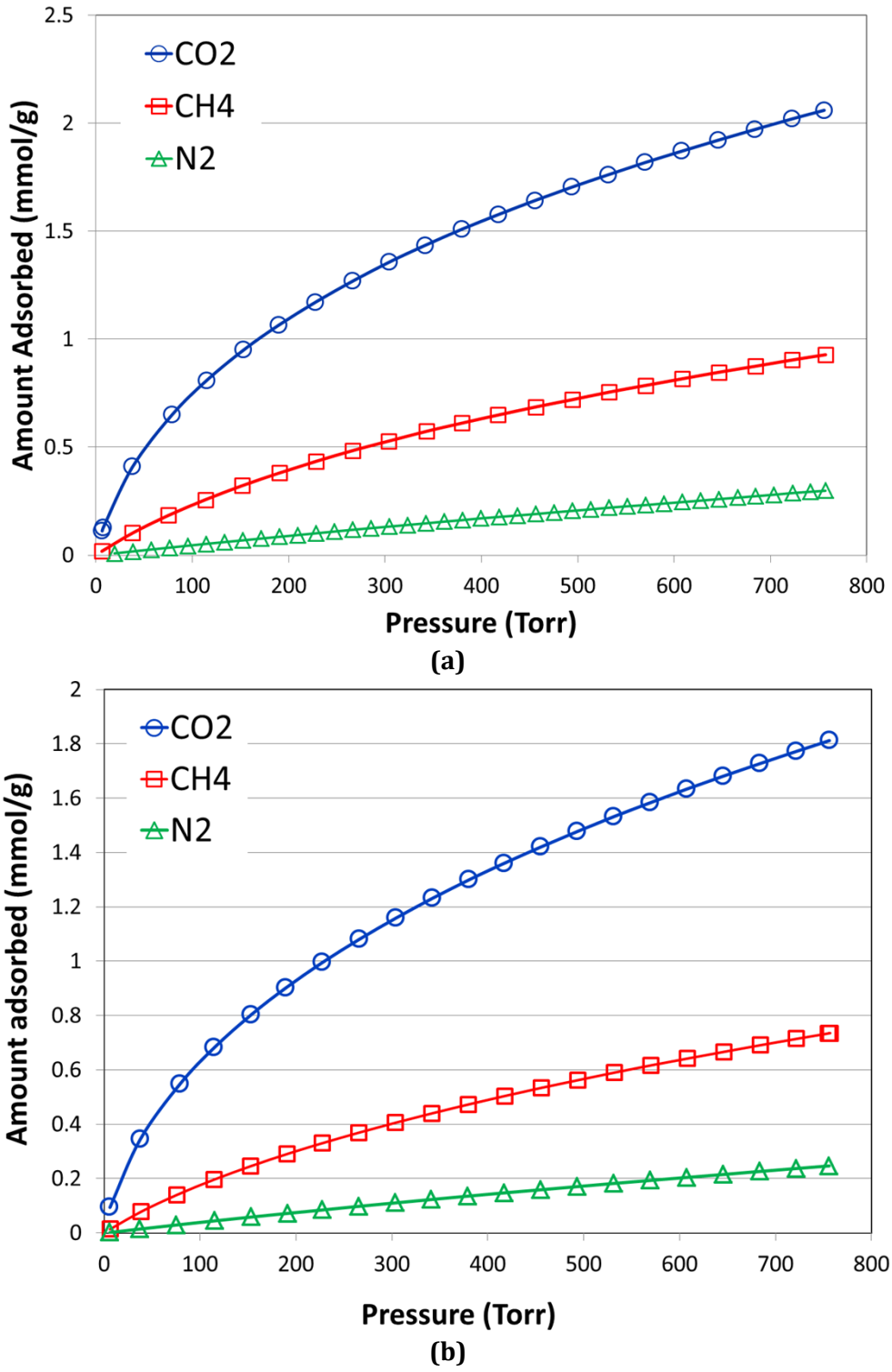

Figure 8. Adsorption isotherms of CO_2, CH_4 and N_2 at 298 K in CS-1 (a) and CS-2 (b)

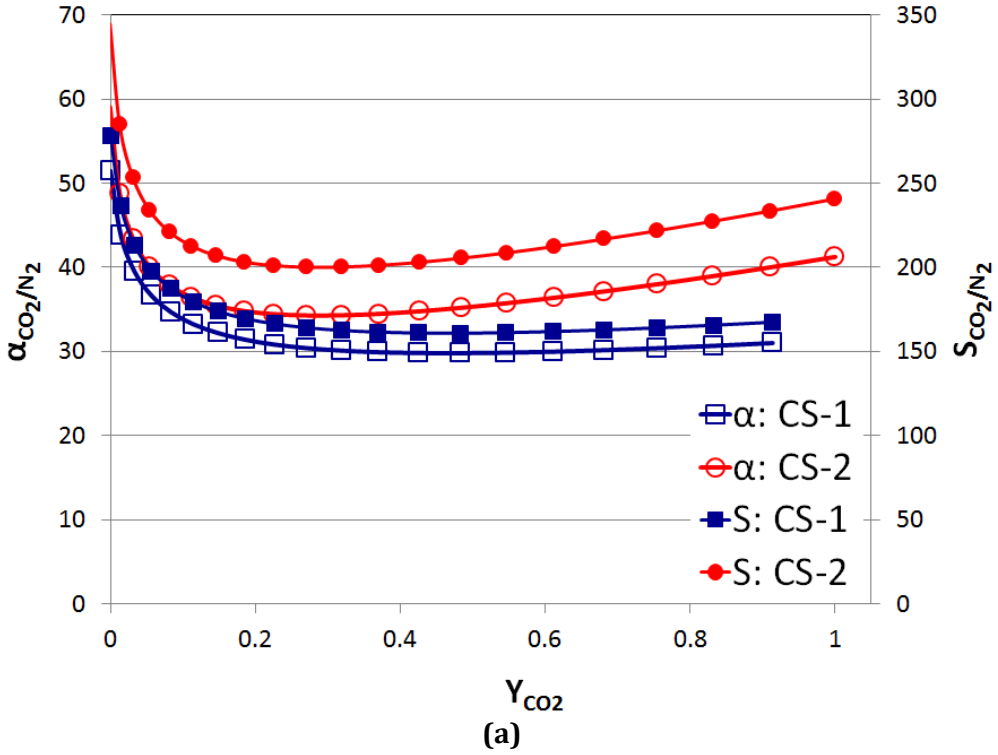

Figure 9. Selectivity (α) and adsorption selection parameter (S) for CO_2/N_2 (a) and CO_2/CH_4 (b) as a function of mole fraction CO_2 (Y_{CO2}) for CS-1 and CS-2

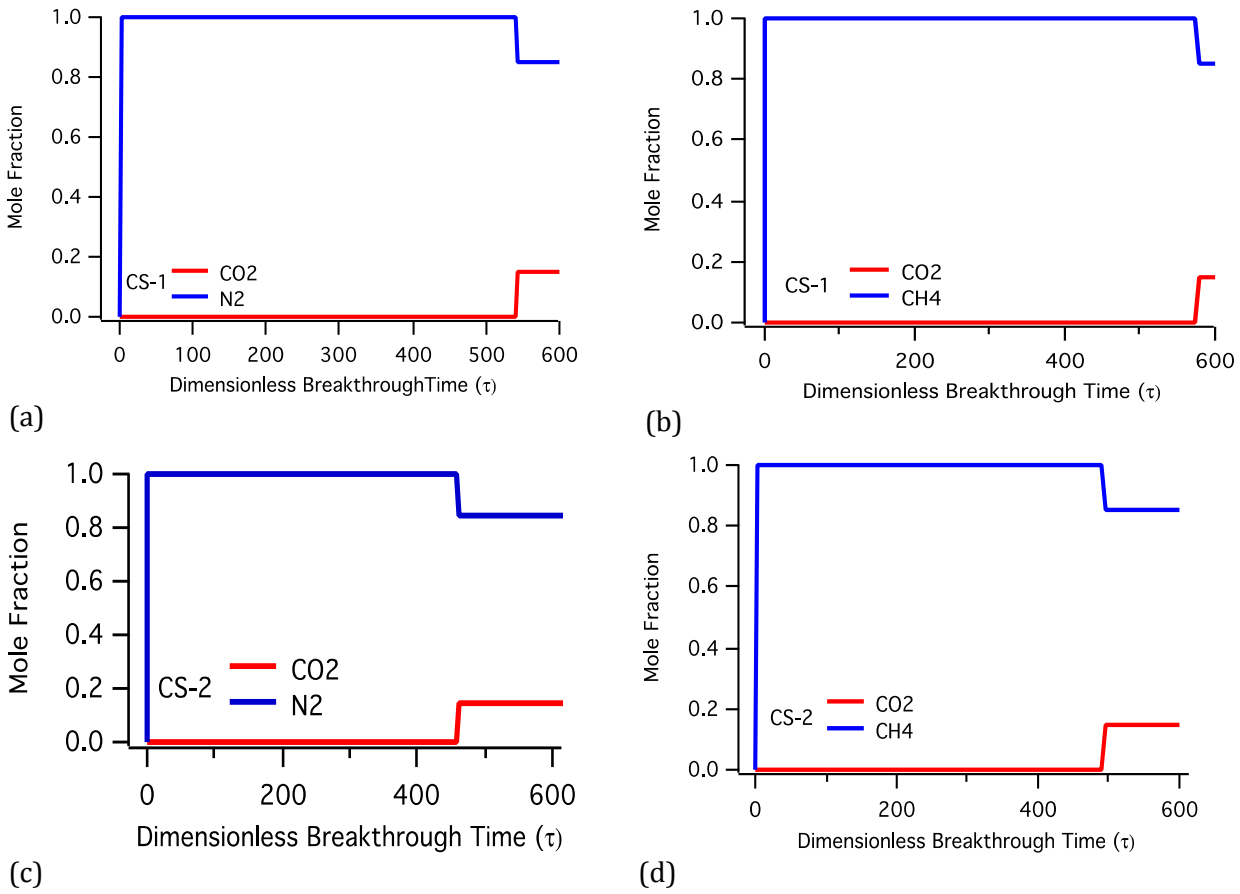

Figure 10. Breakthrough plots for CO_2/N_2 and CO_2/CH_4 in CS-1 and CS-2. Breakthrough time (τ) is represented as, $\tau = \frac{u_o t_{break}}{\varepsilon L}$. All the plots were made with the mole fraction of CO_2 as 0.15 in the feed stream.

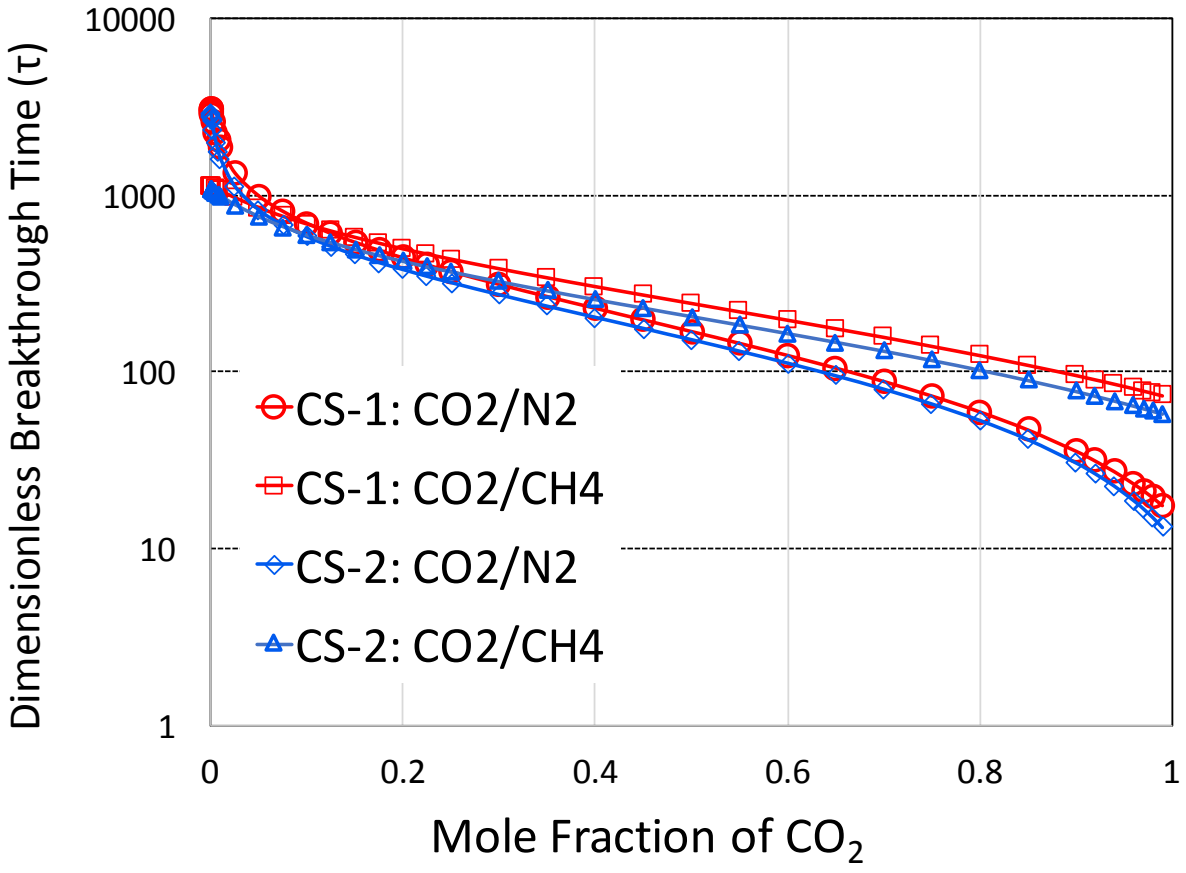

Figure 11. Dimensionless breakthrough time (τ , $\tau = \frac{u_o t_b}{\varepsilon L}$) of CO_2 as a function of its mole fraction in the feed stream

Reference

[1] Haszeldine, R. S. Carbon capture and storage: how green can black be? Science. **2009**, *325*, 1644.

[2] Pachauri, R. K.; Reisinger, A. IPCC Fourth Assessment Report. Intergovernmental Panel on Climate Change, **2007**.

[3] Sumida, K.; Rogow, D. L.; Mason, J. A.; McDonald, T. M.; Blooh, E. D.; Herm, Z. R.; Bae, T-H.; Long, J. R. Carbon Dioxide Capture in Metal–Organic Frameworks. Chem. Rev. **2012**, *112*, 724–781.

[4] Saha, D.; Nelson, K.; Chen. J.; Lu, Y.; Ozcan, S.; Adsorption of Pure and Binary CO_2, CH_4, and N_2 Gas Components on Activated Carbon Beads. J. Chem Data. **2015,** *60*, 2636-2645.

[5] Hao, G-P.; Li, W-C.; Q, D.; Lu, A-H. Rapid Synthesis of Nitrogen-Doped Porous Carbon Monolith for CO2 Capture. Adv. Mater. **2010,** *22*, 853–857.

[6] Saha, D.; Bao, Z.; Jia, F.; Deng, Adsorption of CO2, CH4, N2O, and N2 on MOF-5, MOF-177, and Zeolite 5A. S. Environmental Sci. Technol. **2010**, *44*, 1820-1826.

[7] Siriwardane, R. V.; Shen, M-S.; Fisher, E. P. Adsorption of CO2 on Zeolites at Moderate Temperatures. *Energy Fuels*. **2005**, *19* , 1153–1159.

[8] Cavenati, S.; Grande, C. A.; Rodrigues, A. E. Adsorption Equilibrium of Methane, Carbon Dioxide, and Nitrogen on Zeolite 13X at High Pressures. *J. Chem. Eng. Data*, **2004**, *49* , 1095–1101.

[9] Siriwardane, R. V.; Shen, M-S.; Fisher, E. P. Adsorption of CO2, N2, and O2 on Natural Zeolites. *Energy Fuels*, **2003**, *17*, 571–576.

[10] Kim, W.; Choi, S.; Nair, S. Swelling, functionalization, and structural changes of the nanoporous layered silicates AMH-3 and MCM-22. Langmuir, **2011**, *27*, 7892- 7901.

[11] Zhao, G.; Aziz, B.; Hedin, N. Carbon dioxide adsorption on mesoporous silica surfaces containing amine-like motifs. Applied Energy, **2010**, *87*, 2907–2913.

[12] Belmabkhout, Y.; Serna-Guerrero, R.; Sayari. A.; Adsorption of image from dry gases on MCM-41 silica at ambient temperature and high pressure. 1: Pure image adsorption. Chemical Engineering Science, 2009, *64*, 3721–3728.

[13] D'Alessandro, D.M.; Smit, B.; Long, J.R.; Carbon dioxide capture: Prospects for New Materials. Angew. Chem. Intl. Ed. **2010**, *49*, 6058-6082.

[14] Yong, Z.; Mata, V.; Rodrigues, A. E. Adsorption of carbon dioxide at high temperature—a review. Separation and Purification Technology. **2002,** *26*, 195–205.

[15] Liu, J.; Thallapally, P. K.; McGrail, B. P.; Brown, D. R.; Liua, J. Progress in adsorption-based CO_2 capture by metal–organic frameworks. Chem. Soc. Rev**. 2012**, *41*, 2308-2322

[16] Gargiulo, N.; Pepe, F.; Caputo, D. CO2 adsorption by functionalized nanoporous materials: a review. J. Nanosci. Nanotechnol. **2014**, *14*, 1811-22.

[17] Yu, C-H.; Huang, C-H.; Tan. C-S. A Review of CO_2 Capture by Absorption and Adsorption. Aerosol and Air Quality Research. **2012**, *12*, 745–769.

[18] Choi, S.; Drese, J. H.; Jones, C. W. Adsorbent materials for carbon dioxide capture from large anthropogenic point sources. ChemSusChem. **2009**, *2*, 796-854.

[19] Dai, L.; Xue, Y.; Qu, L.; Choi, H-J.; Baek, J-B. Metal-Free Catalysts for Oxygen Reduction Reaction. Chem. Rev. **2015**, *115*, 4823**–**4892.
[20] Paraknowitsch, J.P.; Thomas, A. Doping carbons beyond nitrogen: an overview of advanced heteroatom doped carbons with boron, sulphur and phosphorus for energy applications. Energy and Environmental Sci **2013**, *6*, 2839-2855.
[21] da Silva, R. R.; Torres, J. H. S.; Kopelevich, Y. Indication of Superconductivity at 35 K in Graphite-Sulfur Composites. Phys. Rev. Lett. **2001**, *87*, 147001.
[22] Kurmaev, E. Z.; Galakhov, A. V.; Moewes, A.; Moehlecke, S.; Kopelevich, Y. Interlayer Conduction Band States in Graphite-Sulfur Composites. Phys. Rev. B. **2002**, *66*, 193402.
[23] Xia, Y.; Zhu, Y.; Tang, Y. Preparation of sulfur-doped microporous carbons for the storage of hydrogen and carbon dioxide. Carbon. **2012**, *50*, 5543–5553..
[24] Seema, H.; Kemp, KC.; Le, NH.; Park, S-W.; Chandra, V.; Lee, JW.; et al. Highly selective CO_2 capture by S-doped microporous carbon materials. Carbon. **2014**, *66*, 320–6.
[25] Bandosz, T. J.; Seredych, M.; Rodríguez-Castellón, E.; Cheng, Y.; Daemen, L. L.; Ramírez-Cuesta, A. J. Carbon. **2016**, *96,* 856**-**863.
[26] Seredych, M.; Jagiello, J.; Bandosz, T. J. Complexity of CO2 adsorption on nanoporous sulfur-doped carbons – Is surface chemistry an important factor? Carbon. **2014**, *74*, 207**–**217.
[27] Liu, X.; Antonietti, M. Moderating Black Powder Chemistry for the Synthesis of Doped and Highly Porous Graphene Nanoplatelets and Their Use in Electrocatalysis. Adv. Mater. **2013**, *25*, 6284-6290.
[28] Saha, D.; Warren, K. E.; Naskar, A. K. Soft-templated mesoporous carbons as potential materials for oral drug delivery. Carbon. **2014**, *71,* 47**–**57.
[29] Saha, D.; Warren, K. E.; Naskar, A. K. Controlled release of antipyrine from mesoporous carbons. Microporous and Mesoporous Materials. **2014**, 196, 327–334.
[30] Saha, D.; Deng, S. Hydrogen Adsorption on Ordered Mesoporous Carbons Doped with Pd, Pt, Ni, and Ru. Langmuir. **2009**, *25*, 12550–12560.
[31] Saha, D.; Deng, S. Adsorption equilibrium and kinetics of CO_2, CH_4, N_2O, and NH_3 on ordered mesoporous carbon. Journal of Colloid and Interface Science. **2010**, *345*, 402–409.
[32] Saha, D.; Moken, T.; Chen, J.; Hensley, D. K.; Delaney, K.; Hunt, M. A.; Nelson, K.; Spurri, A.; Benham, L.; Brice, R.; Azoro, M. Micro-/mesoporous carbons for controlled release of antipyrine and indomethacin. RSC Adv. **2015**, *5*, 23699**–**23707.
[33] Kiciński, W.; Szala, M.; Bystrzejewski, M. Sulfur-doped porous carbons: Synthesis and applications. Carbon. **2014**, *68*, 1**–**32.
[34] Luo, J.; Liu, Y.; Jiang, C.; Chu, W.; Jie, W.; Xie, H. Experimental and Modeling Study of Methane Adsorption on Activated Carbon Derived from Anthracite. J. Chem. Eng. Data. **2011**, *56*, 4919-4926.

[35] D.M. Ruthven, Principles of Adsorption and Adsorption Processes, John Wiley and Sons, ISBN-13: 978-0471866060
[36] Saha, D.; Deng, S. Hydrogen Adsorption on Metal-Organic Framework MOF-177. Tsinghua Sci. Technol. 2010, 15, 363-376.
[37] Yang, R. T. Gas separation by adsorption processes, Imperial College Press, Jan 1, **1997**
[38] Myers, A.L.; Prausnitz, Thermodynamics of mixed gas adsorption, AIChE J. **1965**, *11*, 121-127.

[39] Krishna, R.; van Baten, J.M.; A comparison of the CO_2 capture characteristics of zeolites and metal-organic frameworks Sep. Purif. Technol., **2012**, *87,* 120-126.

[40] Arfken, J. B.; Weber, H. J., Mathematical Methods for Physicists, Academic Press, 2001.

TOC graphic